J|A|C|S ARTICLES

Published on Web 02/05/2010

Resonating Valence Bond and σ-Charge Density Wave Phases in a Benzannulated Phenalenyl Radical

Pradip Bag,[†] Mikhail E. Itkis,[†] Sushanta K. Pal,[†] Bruno Donnadieu,[†] Fook S. Tham,[†] Hyunsoo Park,[‡] John A. Schlueter,[‡] Theo Siegrist,[§] and Robert C. Haddon*[,†]

Departments of Chemistry and Chemical & Environmental Engineering, University of California, Riverside, California 92521-0403, Materials Science Division, Building 200, Argonne National Laboratory, 9700 South Cass Avenue, Argonne, Illinois 60439, and Department of Chemical and Biomedical Engineering, Florida State University, Tallahassee, Florida 32310

Received October 14, 2009; E-mail: haddon@ucr.edu

Abstract: We report the preparation of the first benzannulated phenalenyl neutral radical conductor (**18**), and we show that the compound displays unprecedented solid state behavior: the structure is dominated by two sets of intermolecular interactions: (1) a π-chain structure with superimposed π-overlap of the benzannulated phenalenyls along [0 0 1], and (2) an interchain overlap involving a pair of carbon atoms (C4) along [0 1 0]. The π-chain-type stacking motif is reminiscent of previously reported phenalenyl radicals and the room temperature structure (space group $P2/c$) together with the conductivity of $\sigma_{RT} = 0.03$ S/cm and the Pauli-like magnetic susceptibility are best described by the resonating valence bond (RVB) model. The interchain interaction is unstable with respect to the formation of a σ-charge density wave (σ-CDW) involving pairs of C4 carbon atoms between adjacent radicals and this phase is characterized by the $P2_1/c$ space group which involves a doubling of the unit cell along the [0 1 0] direction. The RVB and CDW phases compete for structural occupancy throughout the whole temperature range (15−293 K) with the RVB phase predominating at 15 and 293 K and the σ-CDW phase achieving a maximum structural occupancy of about 60% at 150 K where it produces clearly discernible effects on the magnetism and conductivity.

Introduction

Most closed shell π-conjugated organic molecules do not form conducting solids owing to their wide HOMO−LUMO gap. Open-shell organic molecules are rare in the solid state, but even in this case it is unusual to obtain conducting solids because of the strength of the on-site Coulomb repulsion which leads to a Mott insulating ground state; thus, most organic molecular conductors are based on charge transfer salts that require electron transfer between two components (donor and acceptor) to generate charge carriers.[1−5]

We have attempted to prepare an intrinsic molecular metal — that is, a solid composed of a single molecular species that would function as a classical (mono) atomic metal and superconductor — such a species is necessarily electron-precise and involves the crystallization of a neutral radical.[6] While we argued in favor of the phenalenyl radical (PLY),[7] the first neutral radical conductors were based on sulfur−nitrogen compounds prepared by Oakley and co-workers.[8−13]

While there has been a great deal of progress in the chemistry of the phenalenyl radical and its derivatives,[14−28] much of our focus has been on multifunctional PLY systems with an emphasis on those in which two PLY units are separated by an

[†] University of California.
[‡] Argonne National Laboratory.
[§] Florida State University.

(1) Garito, A. F.; Heeger, A. J. *Acc. Chem. Res.* **1974**, *7*, 232–240.
(2) Torrance, J. B. *Acc. Chem. Res.* **1979**, *12*, 79–86.
(3) Haddon, R. C. *Acc. Chem. Res.* **1992**, *25*, 127–133.
(4) Williams, J. M.; Ferraro, J. R.; Thorn, R. J.; Carlson, K. D.; Geiser, U.; Wang, H. H.; Kini, A. M.; Whangbo, M.-H. *Organic Superconductors (Including Fullerenes)*; Prentice Hall: Englewood Cliffs, 1992; p 400.
(5) Gunnarsson, O. *Rev. Mod. Phys.* **1997**, *69*, 575–606.
(6) Haddon, R. C. *Aust. J. Chem.* **1975**, *28*, 2343–2351.
(7) Haddon, R. C. *Nature* **1975**, *256*, 394–396.
(8) Oakley, R. T. *Can. J. Chem.* **1993**, *71*, 1775–1784.
(9) Andrews, M. P.; Cordes, A. W.; Douglass, D. C.; Fleming, R. M.; Glarum, S. H.; Haddon, R. C.; Marsh, P.; Oakley, R. T.; Palstra, T. T. M.; Schneemeyer, L. F.; Trucks, G. W.; Tycko, R.; Waszczak, J. V.; Young, K. M.; Zimmerman, N. M. *J. Am. Chem. Soc.* **1991**, *113*, 3559–3568.
(10) Cordes, A. W.; Haddon, R. C.; Oakley, R. T.; Schneemeyer, L. F.; Waszczak, J. V.; Young, K. M.; Zimmerman, N. M. *J. Am. Chem. Soc.* **1991**, *113*, 582–588.
(11) Leitch, A. A.; Reed, R. W.; Robertson, C. M.; Britten, J. F.; Yu, X.; Secco, R. A.; Oakley, R. T. *J. Am. Chem. Soc.* **2007**, *129*, 7903–7914.
(12) Robertson, C. M.; Leitch, A. A.; Cvrkalj, K.; Reed, R. W.; Myles, D. J. T.; Dube, P. A.; Oakley, R. T. *J. Am. Chem. Soc.* **2008**, *130*, 8414–8425.
(13) Hicks, R. G. *Org. Biomol. Chem.* **2007**, *5*, 1321–1338.
(14) Goto, K.; Kubo, T.; Yamamoto, K.; Nakasuji, K.; Sato, K.; Shiomi, D.; Takui, T.; Kubota, M.; Kobayashi, T.; Yakusi, K.; Ouyang, J. *J. Am. Chem. Soc.* **1999**, *121*, 1619–1620.
(15) Morita, Y.; Aoki, T.; Fukui, K.; Nakazawa, S.; Tamaki, K.; Suzuki, S.; Fuyuhiro, A.; Yamamoto, K.; Sato, K.; Shiomi, D.; Naito, A.; Takui, T.; Nakasuji, K. *Angew. Chem., Int. Ed.* **2002**, *41*, 1793–1796.
(16) Fukui, K.; Sato, K.; Shiomi, D.; Takui, T.; Itoh, K.; Gotoh, K.; Kubo, T.; Yamamoto, K.; Nakasuji, K.; Naito, A. *Synth. Met.* **1999**, *103*, 2257–2258.
(17) Takano, Y.; Taniguchi, T.; Isobe, H.; Kubo, T.; Morita, Y.; Yamamoto, K.; Nakasuji, K.; Takui, T.; Yamaguchi, K. *J. Am. Chem. Soc.* **2002**, *124*, 11122–11130.

10.1021/ja908768a

intervening boron atom, although we recently crystallized a trifunctional silicon centered radical (**11**, Scheme 1).[29] The bifunctional compounds are spiro-conjugated at the intervening boron atom so that spin density is delocalized over orthogonal π-systems into two dimensions (**1**−**10**, **12**−**17**, Scheme 1); these compounds address most of the natural objections to neutral radical metals: (a) σ-dimers are rarely observed, (b) the usual 1-dimensional π-stacks are inhibited by the orthogonal geometry of the conjugated systems, (c) they form quarter-filled energy bands and thus avoid the usual insulating charge density wave ground states associated with half-filled bands; furthermore the utilization of quarter-filled bands leads to a much lower ionic fluctuation energy due to the elimination of the on-site Coulomb correlation energy term. A surprising aspect of the solid state structures of these compounds is the absence of charge density wave phases even in the case of the low dimensional compounds.[30−36]

The small energy band gaps exhibited by these solids raises the possibility that it will be possible to close the band gap, stabilize the metallic state and thereby produce intrinsic organic molecular metals and superconductors. While it is difficult to fully account for the electronic structure and solid state properties of the conductors that we have reported, they can be divided into two general classes: (1) narrow band materials where the intermolecular spacing or molecular orientations are such that the overlap between spin-bearing carbon atoms of the molecular unit (which may be composed of a monomer or a dimer) is very poor, and (2) compounds where there is a well established conducting pathway due to the continuous overlap of spin-bearing carbon atoms in 1- or 2-dimensions.[30] We have treated the first class of compounds as Mott-Hubbard insulators,[37−39] whereas we have ascribed the Resonating Valence Bond (RVB) ground state[40,41] to the second group.[30,32,42,43] In both cases, the relevant physics is often treated with the Hubbard model and the Mott-Hubbard transition in solids is governed by the ratio of W/U; where W is the bandwidth and U is the on-site Coulomb repulsion.[44,45]

Scheme 1

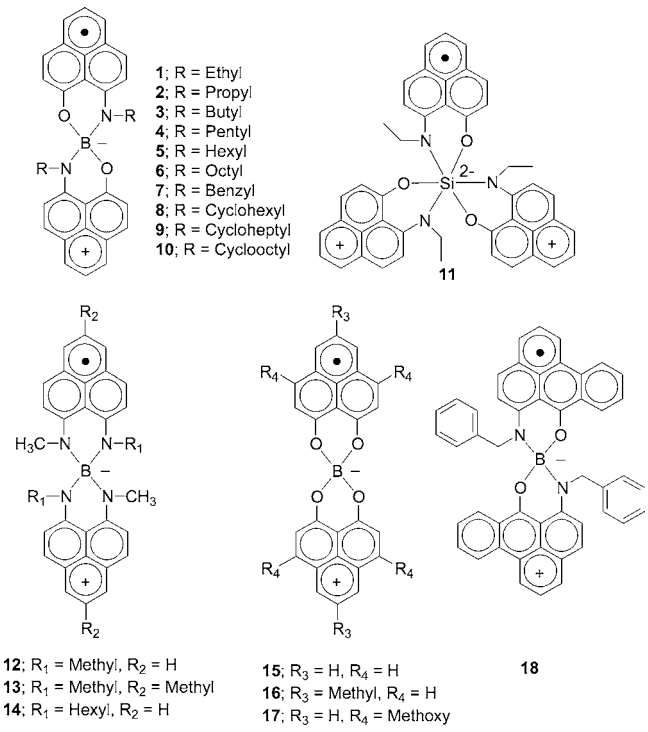

Hence our focus has been on increasing the ratio of W/U and thus we decided to attempt to design a molecule with extended π-conjugation that might both lower the on-site Coulomb repulsion (U), and produce a larger bandwidth (W), while still avoiding the problems associated with 1-D structures and half-filled bands that are characteristic of many planar conjugated π-systems.[1] Thus, we decided to explore a benzannelated derivative of phenalenyl (BPLY), which represents another member of the class of odd alternant hydrocarbons (OAHs).[46] We hoped that at a minimum, the extended π-conjugation would increase the interactions between the molecular orbitals on neighboring lattice sites and hence influence the molecular packing in the solid state.

In the present article, we report the synthesis, electrochemistry, crystallization and characterization of the first member of

(18) Takano, Y.; Taniguchi, T.; Isobe, H.; Kubo, T.; Morita, Y.; Yamamoto, K.; Nakasuji, K.; Takui, T.; Yamaguchi, K. *Chem. Phys. Lett.* **2002**, *358*, 17–23.
(19) Koutentis, P. A.; Chen, Y.; Cao, Y.; Best, T. P.; Itkis, M. E.; Beer, L.; Oakley, R. T.; Brock, C. P.; Haddon, R. C. *J. Am. Chem. Soc.* **2001**, *123*, 3864–3871.
(20) Zheng, S.; Lan, J.; Khan, S. I.; Rubin, Y. *J. Am. Chem. Soc.* **2003**, *125*, 5786–5791.
(21) Zheng, S.; Thompson, J. D.; Tontcheva, A.; Khan, S. I.; Rubin, Y. *Org. Lett.* **2005**, *7*, 1861–1863.
(22) Small, D.; Zaitsev, V.; Jung, Y.; Rosokha, S. V.; Head-Gordon, M.; Kochi, J. K. *J. Am. Chem. Soc.* **2004**, *126*, 13850–13858.
(23) Small, D.; Rosokha, S. V.; Kochi, J. K.; Head-Gordon, M. *J. Phys. Chem. A* **2005**, *109*, 11261–11267.
(24) Zaitsev, V.; Rosokha, S. V.; Head-Gordon, M.; Kochi, J. K. *J. Org. Chem.* **2006**, *71*, 520–526.
(25) Morita, Y.; et al. *Nat. Mater.* **2008**, *7*, 48–51.
(26) Beer, L.; Mandal, S. K.; Reed, R. W.; Oakley, R. T.; Tham, F. S.; Donnadieu, B.; Haddon, R. C. *Cryst. Growth Design* **2007**, *7*, 802–809.
(27) Beer, L.; Reed, R. W.; Robertson, C. M.; Oakley, R. T.; Tham, F. S.; Haddon, R. C. *Org. Lett.* **2008**, *10*, 3121–3123.
(28) Shimizu, A.; Uruichi, M.; Yakushi, K.; Matsuzaki, H.; Okamoto, H.; Nakano, M.; Hirao, Y.; Matsumoto, K.; Kurata, H.; Kubo, T. *Angew. Chem., Int. Ed.* **2009**, *48*, 5482–5486.
(29) Pal, S. K.; Itkis, M. E.; Tham, F. S.; Reed, R. W.; Oakley, R. T.; Haddon, R. *J. Am. Chem. Soc.* **2008**, *130*, 3942–3951.
(30) Haddon, R. C.; Sarkar, A.; Pal, S. K.; Chi, X.; Itkis, M. E.; Tham, F. S. *J. Am. Chem. Soc.* **2008**, *130*, 13683–13690.
(31) Pal, S. K.; Itkis, M. E.; Reed, R. W.; Oakley, R. T.; Cordes, A. W.; Tham, F. S.; Siegrist, T.; Haddon, R. C. *J. Am. Chem. Soc.* **2004**, *126*, 1478–1484.
(32) Pal, S. K.; Itkis, M. E.; Tham, F. S.; Reed, R. W.; Oakley, R. T.; Donnadieu, B.; Haddon, R. C. *J. Am. Chem. Soc.* **2007**, *129*, 7163–7174.
(33) Bohlin, J.; Hansson, A.; Stafstrom, S. *Phys. Rev. B* **2006**, *74*, 155111.
(34) Huang, J.; Kertesz, M. *J. Am. Chem. Soc.* **2003**, *125*, 13334–13335.
(35) Huang, J.; Kertesz, M. *J. Am. Chem. Soc.* **2006**, *128*, 1418–1419.
(36) Huang, J.; Kertesz, M. *J. Am. Chem. Soc.* **2007**, *129*, 1634–1643.
(37) Chi, X.; Itkis, M. E.; Patrick, B. O.; Barclay, T. M.; Reed, R. W.; Oakley, R. T.; Cordes, A. W.; Haddon, R. C. *J. Am. Chem. Soc.* **1999**, *121*, 10395–10402.
(38) Chi, X.; Itkis, M. E.; Kirschbaum, K.; Pinkerton, A. A.; Oakley, R. T.; Cordes, A. W.; Haddon, R. C. *J. Am. Chem. Soc.* **2001**, *123*, 4041–4048.
(39) Chi, X.; Itkis, M. E.; Reed, R. W.; Oakley, R. T.; Cordes, A. W.; Haddon, R. C. *J. Phys. Chem. B* **2002**, *106*, 8278–8287.
(40) Anderson, P. W. *Mater. Res. Bull.* **1973**, *8*, 153–160.
(41) Pauling, L. *Nature* **1948**, *161*, 1019–1020.
(42) Mandal, S. K.; Samanta, S.; Itkis, M. E.; Jensen, D. W.; Reed, R. W.; Oakley, R. T.; Tham, F. S.; Donnadieu, B.; Haddon, R. C. *J. Am. Chem. Soc.* **2006**, *128*, 1982–1994.
(43) Pal, S. K.; Itkis, M. E.; Tham, F. S.; Reed, R. W.; Oakley, R. T.; Haddon, R. C. *Science* **2005**, *309*, 281–284.
(44) Anderson, P. W. *Science* **1987**, *235*, 1196–1198.
(45) Powell, B. J.; McKenzie, R. H. *J. Phys.: Condens. Matter.* **2006**, *18*, R827–R866.
(46) Haddon, R. C. *Aust. J. Chem.* **1982**, *35*, 1733–1738.

Scheme 2

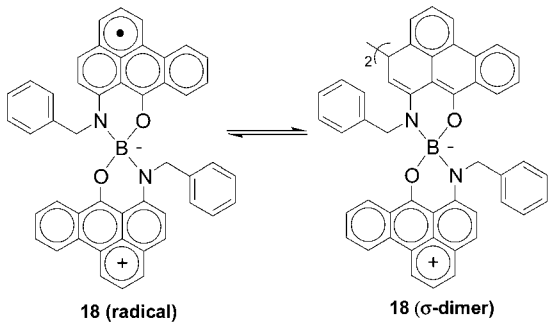

a new family of spiro-bis(6,7-disubstituted benzannelated phenalenyl) boron neutral radicals (**18**, Scheme 1); detailed analysis of the solid state properties shows that a σ-bonded dimer and a stacked π-chain radical coexist and interconvert in the crystal as a solid solution which forms the basis for competing resonating valence bond (RVB) and σ-charge density wave (σ-CDW) phases in crystalline **18** (Scheme 2). The σ-CDW is an unusual case of the charge density wave ground state that is characteristic of low-dimensional metals, in which the charge density is periodically modulated due to σ-bond formation with a period (in our case), of twice the lattice constant of the undistorted structure (see below).

Results and Discussion

Synthesis of Benzannelated Phenalenyl Derivatives. The previous synthesis of 6-hydroxy-7-oxo-benzanthracene (**19**) made use of a two step procedure to isolate the desired compound;[46] the first step involved the Friedel−Crafts acylation of 2-methoxynaphthalene with benzoyl chloride to prepare (2-methoxy-naphthalen-1-yl)-phenyl-methanone, whereas the second step required Scholl conditions to couple the aromatic rings. The harsh Scholl reaction conditions resulted in a difficult workup and low yields (<12%), and this prompted the investigation of other synthetic routes. By utilizing a modified Scholl reaction (Scheme 3), we were able to increase the yield of the reaction to ~60%, without the necessity of isolating intermediate products; 6-*N*-benzylamino-7-oxo-benzanthracene (**20**) was prepared in high yield by treating the hydroxy derivative (**19**) with benzyl amine in a sealed tube.

Preparation and Electrochemical Properties of Radical 18. The synthesis of radical **18** followed the same basic principle that has been applied to prepare previous phenalenyl-based neutral radicals.[37,38] We first prepared the chloride salt (**18**$^+$ Cl^-) by reacting **20** with boron trichloride and then exchanged the counteranion with tetraphenyl borate to achieve the required solubility properties of the salt (Scheme 4). The electrochemical characteristics of **18**$^+$ BPh_4^- were examined by cyclic voltammetry and differential pulse voltammetry and it may be seen in Figure 1 that there are two reversible redox couples with half-wave potentials: $E_1^{1/2} = -0.81$ V and $E_2^{1/2} = -1.17$ V. Each of these redox couples corresponds to a one-electron reduction process, indicating successive generation of radical and anion (Scheme 5). The disproportionation potential between these two redox couples, $\Delta E_{2-1} = E_2^{1/2} - E_1^{1/2} = -0.36$ V, is slightly more negative than that of the corresponding phenalenyl analog ($\Delta E_{2-1} = -0.33$ V),[31] and thus the extended π-conjugation does not reduce the value of $|\Delta E_{2-1}|$, although other approaches have been successful in this regard.[47]

We crystallized the radical **18** by the use of a chemical reductant (Scheme 4) in a H -cell and obtained a moderate yield of high quality crystals. The salt **18**$^+$ BPh_4^- can be reduced by

Scheme 3

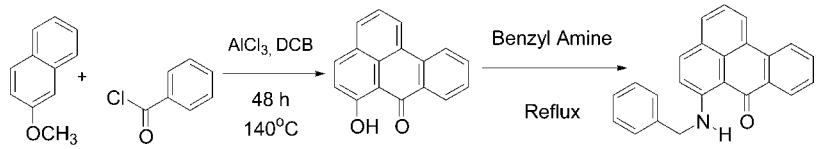

Scheme 4

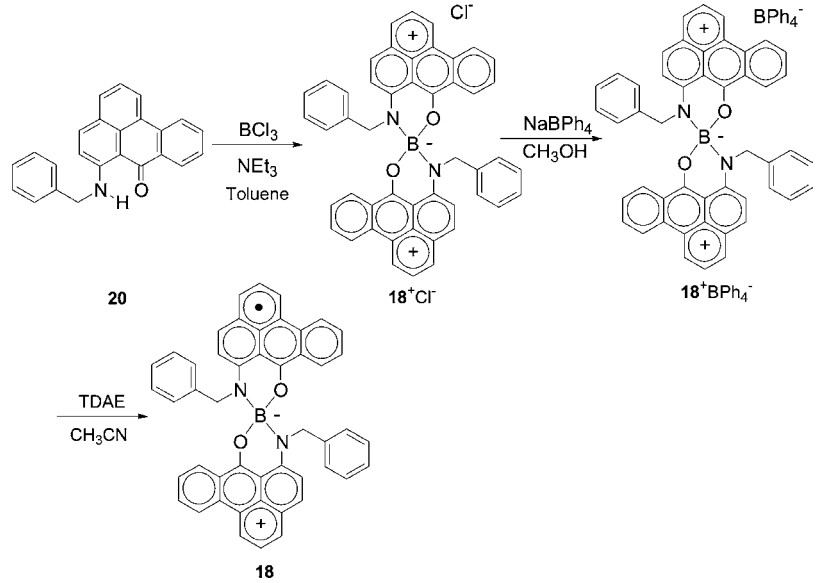

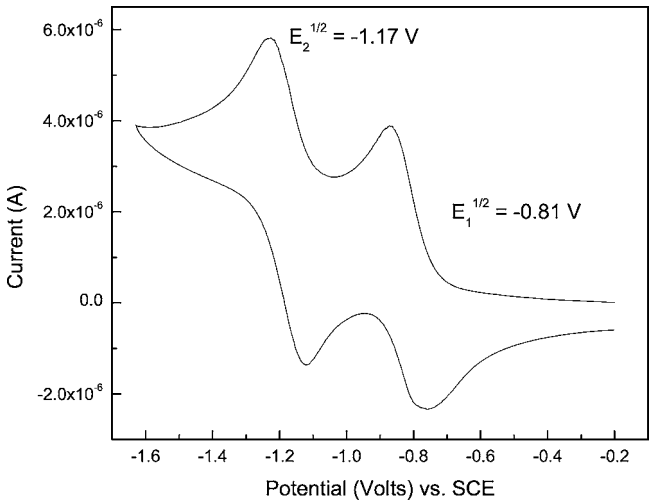

Figure 1. Cyclic voltammetry of $\mathbf{18}^{+}$ BPh_4^- in acetonitrile, referenced to SCE via internal ferrocene (not shown).

Scheme 5

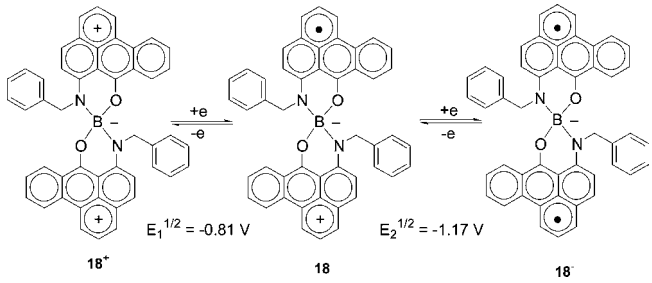

using cobaltocene ($E^{1/2} = -0.91$ V vs SCE),[48] but the reduction process is fast and the crystals are small. However, the use of tetrakis(dimethylamino)ethylene (TDAE, $E^{1/2} = -0.75$ V vs SCE),[49] leads to a slower reduction and much better radical crystals can be obtained. The crystals reached their optimum size and quality in two weeks. Although solutions of the radical are extremely oxygen sensitive, the crystals are stable enough to obtain elemental analysis, X-ray crystal structures, and other solid state measurements under ambient condition.

Structural Analysis of 18. The radical (**18**) was obtained as black, shining crystals which were structurally characterized at 14 temperatures between 15 and 293 K (crystal parameters are given in Table S3, S4, Supporting Information). Six of the carbon atoms have high thermal parameters throughout the full temperature range: C4 (C24), and their directly bonded neighbors, and detailed analysis of the crystallographic information shows that a σ-bonded dimer and a stacked π-chain radical coexist and interconvert in the crystal as a solid solution which forms the basis for competing resonating valence bond (RVB) and σ-charge density wave (σ-CDW) ground states in crystalline **18** (Scheme 2, Figures 2 and 3).

The analysis of the radical structure and its superstructure is discussed in detail in the Supporting Information and in what follows we briefly summarize our main findings. Room temperature X-ray measurements indicated the monoclinic space

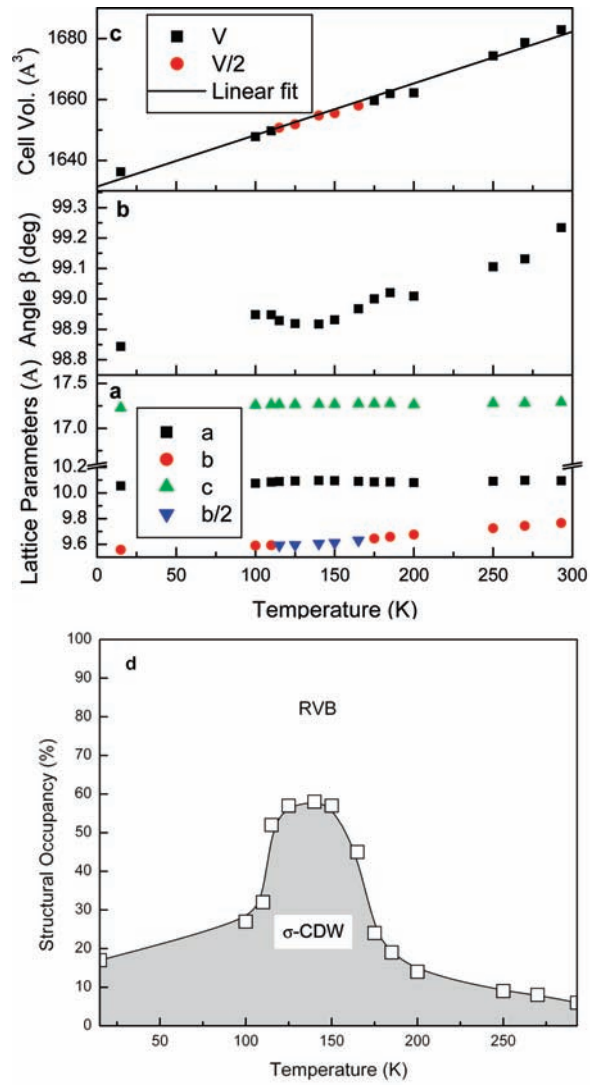

Figure 2. Structural parameters as a function of temperature: (a) lattice parameters a, b, c; note the doubling of b from 115 to 165 K. (b) Lattice parameter β; (c) cell volume (V); note the doubling of V from 115 to 165 K. (d) Structural occupancy of RVB and σ-CDW phases.

group $P2/c$, with the boron atom sitting on the 2-fold axis; thus the asymmetric unit contains half of the molecule. In the RVB structure the unpaired electron is fully delocalized (radical) and the two halves of the molecule remain identical and this structure is accommodated by the $P2/c$ space group. Superstructure reflections are visible at all temperatures and suggest a doubling of the unit cell along the [0 1 0] direction and at temperatures in the vicinity of 150 K, the observed space group becomes $P2_1/c$. Since each molecule of **18** contains one unpaired electron, the local symmetry must be lowered to correctly describe σ-bond formation; thus for the superstructure, the same arrangement remains, but half of the end-to-end contacts now form σ-dimers, thereby localizing the spins in the σ-bond between a pair of molecules. This displacive superstructure is reflected in the doubling of the unit cell along the b-axis, and a lowering of the apparent symmetry to $P2_1/c$. The relative population of the phases [π-chain-RVB radical ($P2/c$) and σ-dimer-CDW ($P2_1/c$)] in the crystal shows an extremely unusual temperature dependence (Figure 2d): the fraction of the σ-dimer-CDW phase increases as the temperature is lowered, reaches a broad maximum in the interval between 165 and 115 K, and then

(47) Sarkar, A.; Pal, S. K.; Itkis, M. E.; Liao, P.; Tham, F. S.; Donnadieu, B.; Haddon, R. C. *Chem. Mater.* **2009**, *21*, 2226–2237.
(48) Robbins, J. L.; Edelstein, N.; Spencer, B.; Smart, J. C. *J. Am. Chem. Soc.* **1982**, *104*, 1882–1893.
(49) Kolomeitsev, A.; Medebielle, M.; Kirsch, P.; Lork, E.; Roschenthaler, G.-V. *J. Chem. Soc., Perkin Trans. 1* **2000**, 2183–2185.

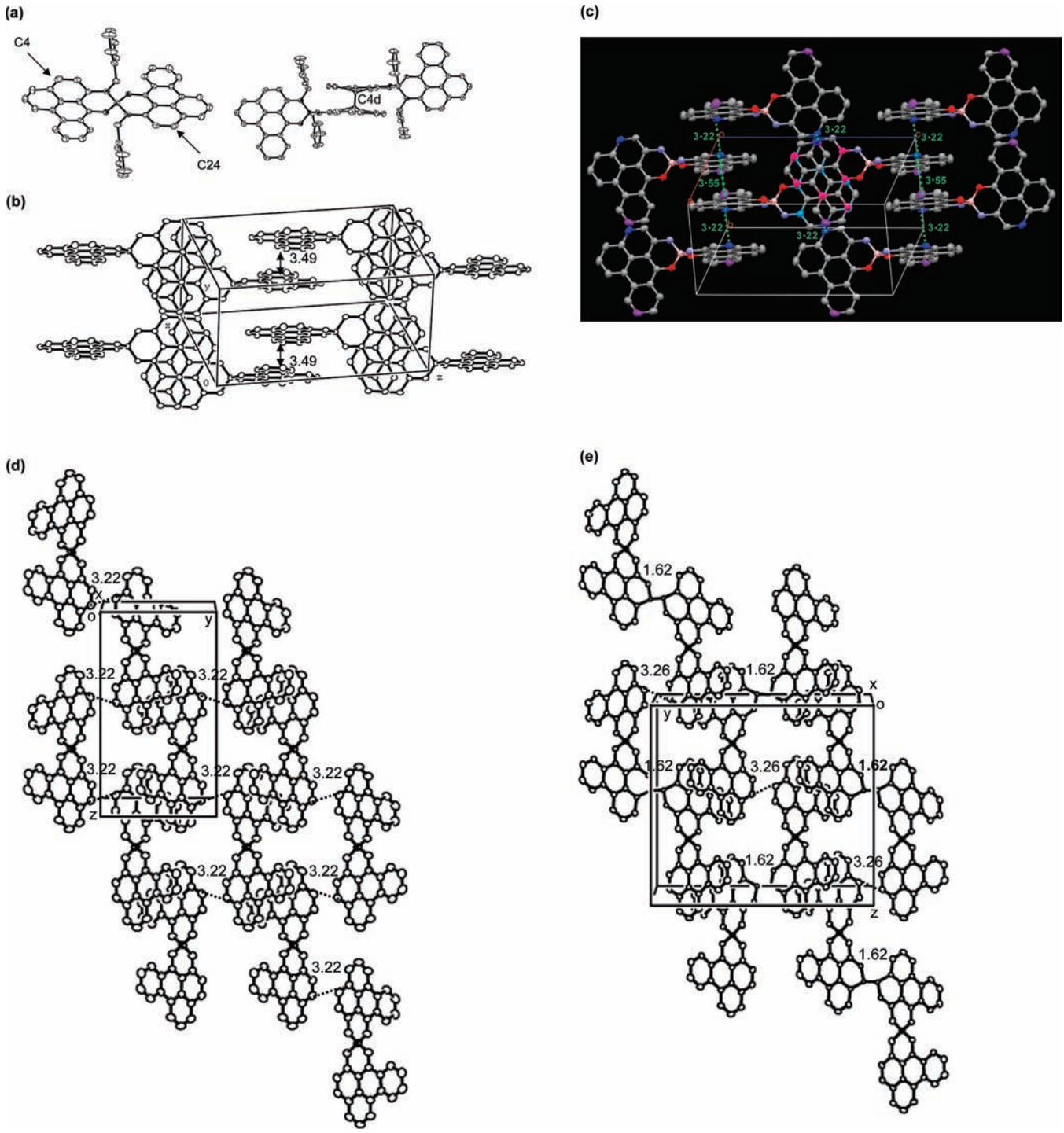

Figure 3. (a) ORTEP drawing of radical **18** showing the carbon atoms with close interchain contacts (293 K), and the σ-dimer which forms by bonding of C4(C24) pairs of atoms (150 K). (b) Unit cell of crystalline **18**, at 293 K, showing the packing along the *z*-axis viewed normal to one of the benzannulated phenalenyl planes (benzyl groups omitted); the interplanar separation of 3.49 Å between π-stacked BPLY units is shown. (c) Packing of the molecules in the crystal lattice of **18** at 293 K, showing the dual roles played by the C4 (blue) carbon atoms in the radical form: C4···C4 = 3.22 Å, C4···C10 (purple) = 3.55 Å, (benzyl groups omitted); the internuclear separation of 3.22 Å between the C4···C4 pairs of atoms and the overlap of six spin bearing carbon atoms in adjacent BPLY units are evident. (d) X-ray structure of **18** at 293 K (RVB phase), showing the close contact along the *y*-axis, the C4···C4 = C24···C24 contacts are uniform throughout the crystal lattice (benzyl groups omitted). (e) X-ray structure of **18** at 150 K (σ-Dimer phase), showing the close contact (C24···C24) along *y*-axis together with the formation of the σ-bond (C4d−C4d), (benzyl groups omitted).

decreases monotonically as the temperature is lowered to 15 K (Table 1, Figure 2).

The radicals pack in a spiro-conjugated π-chain along the z-direction and within this chain the carbon···carbon distances are in the range 3.47−3.55 Å (293 K); the packing of the molecules reveals that the BPLY units of nearest neighbor molecules are parallel to each other and are involved in superimposed π-overlap (Figure 3b) between six pairs of spin-bearing carbon atoms (out of a total of eight) in each BPLY unit. This configuration minimizes the steric interference and

Table 1. Crystal Data of **18** for All Temperatures

	Temp.													
	15 K	100 K	110 K	115 K	125 K	140 K	150 K	165 K	175 K	185 K	200 K	250 K	270 K	293 K
Space group	*P*2/*c*	*P*2/*c*	*P*2/*c*	$P2_1/c$	$P2_1/c$	$P2_1/c$	$P2_1/c$	$P2_1/c$	*P*2/*c*	*P*2/*c*	*P*2/*c*	*P*2/*c*	*P*2/*c*	*P*2/*c*
a, Å	10.0564(4)	10.0768(4)	10.0850(3)	10.0893(4)	10.0928(4)	10.0971(3)	10.0955(3)	10.0904(3)	10.0865(3)	10.0856(3)	10.0785(4)	10.0913(5)	10.0982(10)	10.096(2)
b, Å	9.5585(4)	9.5915(4)	9.5920(3)	19.1848(7)	19.1906(7)	19.2119(6)	19.2247(6)	19.2620(6)	9.6443(3)	9.6576(3)	9.6735(4)	9.7249(5)	9.7433(10)	9.766(2)
c, Å	17.2269(7)	17.2589(6)	17.2635(5)	17.2652(6)	17.2656(6)	17.2693(6)	17.2688(6)	17.2721(5)	17.2734(5)	17.2759(5)	17.2616(7)	17.2789(8)	17.2806(17)	17.292(4)
β, degree	98.8441(18)	98.9481(4)	98.9476(4)	98.9288(6)	98.9185(2)	98.9174(5)	98.9312(5)	98.9678(5)	98.9999(5)	99.0203(4)	99.0046(7)	99.1054(8)	99.1317(16)	99.234(3)
V, Å^3	1636.23(12)	1647.80(11)	1649.67(9)	3301.40(2)	3303.70(6)	3309.48(18)	3310.94(18)	3315.99(17)	1659.62(9)	1661.91(9)	1662.17(12)	1674.33(14)	1678.70(3)	1682.9(6)
Z	2	2	2	4	4	4	4	4	2	2	2	2	2	2
% disorder (C4/C4d)	83/17	73/27	68/32	48/52	43/57	42/58	43/57	55/45	76/24	81/19	86/14	91/9	92/8	94/6
C4···C4, Å	3.187(5)	3.223(5)	3.232(5)	3.184(13)	3.182(14)	3.175(15)	3.188(12)	3.194(10)	3.230(4)	3.222(4)	3.217(4)	3.222(4)	3.223(4)	3.223(3)
% disorder (C24/C24d)				82/18	86/14	91/9	93/7	90/10						
C24···C24, Å				3.252(4)	3.255(4)	3.259(4)	3.259(3)	3.252(4)						
C24d−C24d, Å				1.622(10)	1.620(10)	1.618(10)	1.620(10)	1.621(10)						
R1-value	4.82	4.65	4.68	7.94	6.88	6.06	5.96	5.95	4.57	4.52	4.66	4.54	4.49	4.61

maximizes the overlap between the singly occupied molecular orbitals (SOMOs) of the adjacent BPLY units. By repeating this superimposed π-overlap, the radical forms a highly symmetrical π-chain structure along the [0 0 1] direction (Figure 3b). The π-chain (z) axis corresponds to the needle axis of the crystal. Thus the solid-state packing of radical **18** is very similar to that observed for phenalenyl-based radical **8**,[43] **9**,[32] **15** and **16**,[42] which form a highly symmetrical π-chain-type structure by repeating the superimposed π-overlap along the [1 0 1] direction with slightly shorter intermolecular C···C distances.

The crystal packing of radical **18** shows a short set of interchain C···C contacts along the *y*-axis involving the spin-bearing carbons C4 and C24 of the BPLY rings; it is important to note that these carbon atoms are involved in both of the strong interactions in the crystal (Figure 3a and c). In the RVB phase (Figure 3d) they are just one of the six spin bearing carbon atoms on each BPLY involved in the π-chain, whereas in the CDW phase (Figure 3e) one of them becomes involved in σ-dimer formation which serves to localize all of the spin density at a single atom (C4 or C24); based on an HMO analysis of BPLY, this carbon does not possess the highest spin density and it seems likely that the radicals dimerize at these positions due to their proximity in the solid state structure and thus the mode of dimerization is governed by the packing of the radicals in the crystal lattice. The molecular packing of **18** in the CDW phase (Figure 3e) shows that one end of the molecule is involved in σ-dimer formation while the other end of the molecule is still in the π-overlap with its neighbor in the π-chain and the interplanar separation varies from 3.43−3.45 Å. In the CDW phase the C4 carbon atom deviates from the mean plane by 0.75 Å and forms a C4d-C4d σ-bond of length 1.62 Å indicating a change in hybridization from sp^2 to sp^3; the C−C σ-bond distance is comparable with that found in other σ-dimerized

(50) Miller, J. S.; Zhang, J. H.; Reiff, W. M.; Dixon, D. A.; Preston, L. D.; Reis, A. H.; Gebert, E.; Extine, M.; Troup, J.; Epstein, A. J.; Ward, M. D. *J. Phys. Chem.* **1987**, *91*, 4344–4360.
(51) Kahr, B.; Engen, D. V.; Mislow, K. *J. Am. Chem. Soc.* **1986**, *108*, 8305–8307.
(52) Kaupp, G.; Boy, J. *Angew. Chem., Int. Ed.* **1997**, *36*, 48–49.
(53) Liao, P.; Itkis, M. E.; Oakley, R. T.; Tham, F. S.; Haddon, R. C. *J. Am. Chem. Soc.* **2004**, *126*, 14297–14302.
(54) Yoldi, I. G.; Miller, J. S.; Novoa, J. J. *J. Phys. Chem. A* **2009**, *113*, 7124–7132.
(55) Vazquez, C.; Calabrese, J. C.; Dixon, D. A.; Miller, J. S. *J. Org. Chem.* **1993**, *58*, 65–81.
(56) Novoa, J. J.; Lafuente, P.; Del Sesto, R. E.; Miller, J. S. *Angew. Chem., Int. Ed.* **2001**, *40*, 2540–2543.
(57) Jung, D.-H.; Kim, B. H.; Ko, Y. K.; Jung, M. S.; Jung, S.; Lee, S. Y.; Jung, H.-T. *Langmuir* **2004**, *20*, 8886–8891.
(58) Reed, C. A.; Bolskar, R. D. *Chem. Rev.* **2000**, *100*, 1075–1120.
(59) Miller, J. S.; Novoa, J. J. *Acc. Chem. Res.* **2007**, *40*, 189–196.
(60) Konarev, D. V.; Khasanov, S. S.; Saito, G.; Otsuka, A.; Yoshida, Y.; Lyubovskaya, R. N. *J. Am. Chem. Soc.* **2003**, *125*, 10074–10083.
(61) Konarev, D. V.; Khasanov, S. S.; Otsuka, A.; Saito, G. *J. Am. Chem. Soc.* **2002**, *124*, 8520–8521.
(62) Rao, A. M.; Zhou, P.; Wang, K. A.; Hager, G. T.; Holden, J. M.; Wang, Y.; Lee, W. T.; Bi, X.-X.; Eklund, P. C.; Cornett, D. S.; Duncan, M. A.; Amster, I. J. *Science* **1993**, *259*, 955–957.
(63) Haddon, R. C. *Science* **1993**, *261*, 1545–1550.
(64) Haddon, R. C.; Chow, S.-Y. *J. Am. Chem. Soc.* **1998**, *120*, 10494–10496.
(65) Morosin, B.; Plastas, H. J.; Coleman, L. B.; Stewart, J. M. *Acta Crystallogr.* **1978**, *B34*, 540–543.
(66) Hoffmann, S. K.; Corvan, P. J.; Singh, P.; Sethulekshmi, C. N.; Metzger, R. M.; Hatfield, W. E. *J. Am. Chem. Soc.* **1983**, *105*, 4608–4617.
(67) Radhakrishnan, T. P.; Engen, D. V.; Soos, Z. G. *Mol. Cryst. Liq. Cryst.* **1987**, *150b*, 473–492.
(68) Zhao, H.; Heintz, R. A.; Ouyang, X.; Dunbar, K. R.; Campana, C. F.; Rogers, R. D. *Chem. Mater.* **1999**, *11*, 736–746.

π-systems.[25,32,50−54] There are a number of other dimers with very short $\pi-\pi$ contacts,[55−59] but few of these interactions actually collapse to a full σ-bond[25,60,61] and with the exception of the fullerenes[62] and fullerides,[60,61] we are not aware of any system in which a σ-CDW competes with a conducting state. The fullerenes must be considered as a special cases of σ-CDW formation because the necessary rehybridization is already built into the undimerized structure: thus the value of the pyramidalization angle (θ_P) in a normal π-system is $\theta_P = 0°$, whereas the value in C_{60} is $\theta_P = 11.6°$ — well on the way to the standard tetrahedral value of $\theta_P = 19.5°$.[63,64]

Although σ-dimers are occasionally observed in systems such as those containing the tetracyanoquinodimethane (TCNQ) anion,[54,65−68] none of these derive from a high symmetry conducting state and only one of these cases shows reversible σ-bond formation and even here the transition is strongly hysteretic.[67] The parent phenalenyl radical is presumed to undergo σ-dimerization which eventually leads to peropyrene,[69] and this behavior has recently been observed in a methoxy-substituted derivative.[26] Two spiro-biphenalenyl radicals have been crystallized as both σ- and π-dimers by appropriate control of the occurrence domain of the crystallization event,[32,53] although they do not undergo interconversion; recently a diazaphenalenyl radical has been shown to exist as an equilibrating mixture of σ- and π-dimers in the solid state.[25]

Magnetic Susceptibility and Conductivity of Radical 18. The magnetic susceptibility (χ) of **18** was measured over the temperature range 4 to 360 K, and is shown in Figure 4a as the paramagnetic susceptibility (χ_p, after diamagnetic correction); between 190 to 360 K, crystalline **18** shows a temperature independent paramagnetic susceptibility $\chi_p = 545 \times 10^{-6}$ emu mol^{-1}, which is similar to the Pauli paramagnetism seen in the phenalenyl-based neutral radicals **8** and **9** (Figure 4a) and is typical of the values obtained for other molecular metals and superconductors.[43,70,71] Below 190 K the paramagnetic susceptibility decreases and reaches a minimum value of 260×10^{-6} emu mol^{-1} at about 130 K, a decrease in paramagnetism of over 50%. Below 130 K it again starts to increase and the Curie tail observed below 100 K arises from the presence of residual paramagnetic centers in the lattice — the concentration of which is considerably greater than the values typically found for phenalenyl radical conductors;[32,43] the origin of the high spin count is attributed to trapped solitons and further discussed below.

The single crystal electrical conductivity of **18** was measured on two single crystals (see Supporting Information) using four-point contacts along the needle (z) axis (Figure 4c), and the temperature dependence of the conductivity is shown in Figure 4d. The value of the room temperature conductivity is $\sigma_{RT} = 0.03$ S/cm and it is apparent that there are at least two different conduction regimes. The conductivity shows semiconducting temperature dependence with activation energies of 0.11 and 0.55 eV; the fine scale analysis in Figure 4b shows that the activation energy of the conductivity reaches a maximum at ~150 K.

Band Electronic Structure of 18. The extended Hückel (EHT) band structure and the density of states (DOS) calculations

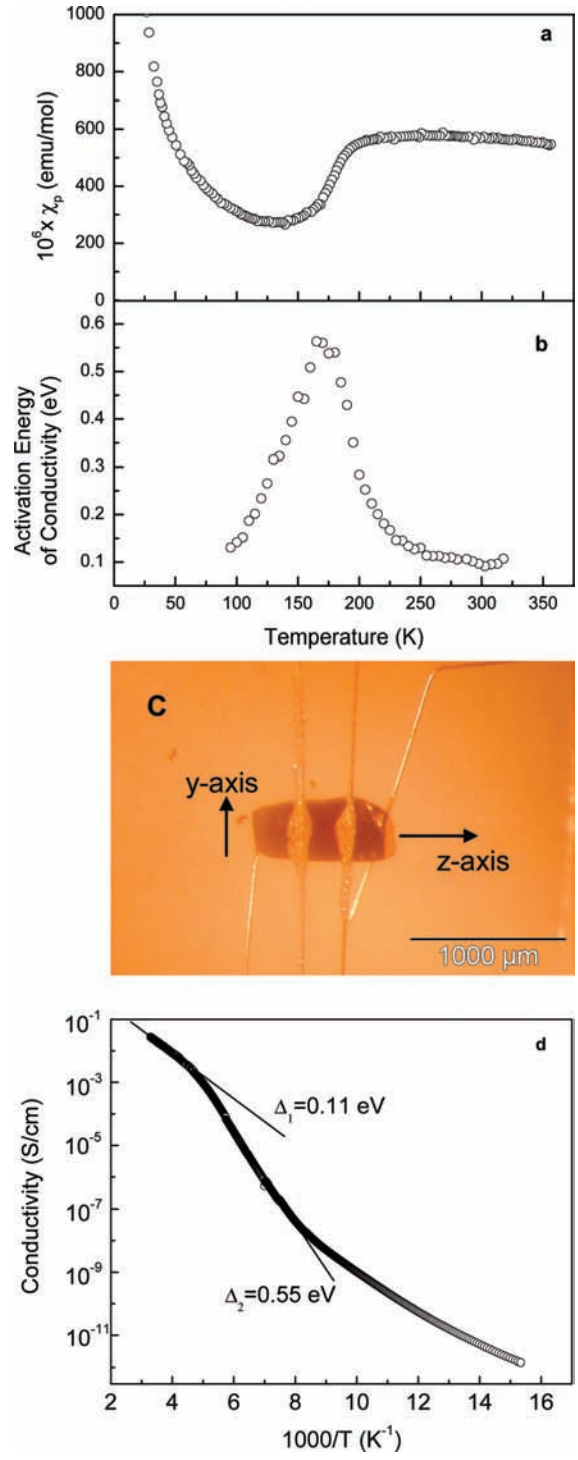

Figure 4. (a) Magnetic susceptibility. (b) Activation energy of the conductivity of crystalline **18**. (c) Picture of crystal wired for 4-probe conductivity measurement, showing the needle axis. (d) Single-crystal conductivity of crystalline **18** as a function of reciprocal temperature (T).

(Experimental Section) of the RVB structure at 293 K and the σ-CDW structure at 150 K are presented in Figure 5. The four bands shown in Figure 5a for the 293 K structure are derived from the two lowest unoccupied molecular orbitals (LUMOs) of the cation $\mathbf{18}^+$, for each of the two molecules of **18** in the unit cell ($P2/c$ space group). Basically, these consist of the symmetric and antisymmetric combinations of the BPLY LUMOs; alternatively they can be viewed as arising from the

(69) Reid, D. H. *Quart. Rev.* **1965**, *19*, 274–302.
(70) Haddon, R. C.; Ramirez, A. P.; Glarum, S. H. *Adv. Mater.* **1994**, *6*, 316–322.
(71) Murata, T.; Morita, Y.; Fukui, K.; Sato, K.; Shiomi, D.; Takui, T.; Maesato, M.; Yamochi, H.; Saito, G.; Nakasuji, K. *Angew. Chem. Int. Ed* **2004**, *43*, 6343–6346.

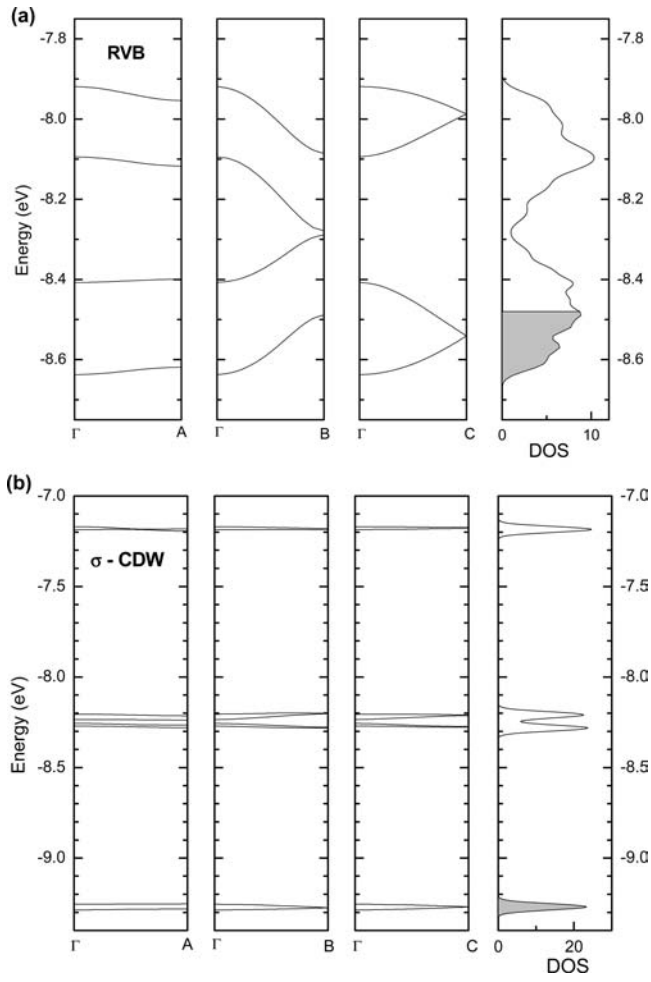

Figure 5. EHT band structure and DOS calculated for the experimental structures of crystalline **18**: (a) RVB structure at 293 K (space group $P2/c$, $z = 2$), (b) σ-CDW structure at 150 K (space group $P2_1/c$, $z = 4$). Where $\Gamma = 0, 0, 0$; $A = 1/2, 0, 0$; $B = 0, 1/2, 0$; $C = 0, 0, 1/2$, and the coordinates are given in units of the reciprocal lattice vectors; the shaded region indicates the occupied states.

nonbonding molecular orbitals of each of the four BPLY units in the unit cell. In the radical phase of **18** the orbitals in Figure 5a accommodate a total of two electrons, leading to a quarter-filled band complex and a finite DOS at the Fermi level suggesting metallic character in the RVB state. The maximum dispersion along the π-chain in **18** has a value of 0.23 eV ($T =$ 293 K), which may be compared with values of 0.20 eV (**8**, 297 K) and 0.22 eV (**9**, 273 K); the mean plane separations are: 3.32 Å (**8**), 3.31 Å (**9**), and 3.48 Å (**18**), and thus according to the EHT calculations, the BPLY π-system is more effective than PLY in enhancing the bandwidths of the π-chain compounds.

In the 150 K band structure (Figure 5b), the unit cell has doubled in size (space group $P2_1/c$) so as to accommodate four molecules (two σ-dimers) which give rise to 8 orbitals occupied by 4 electrons; the large energy gap between the valence and conduction bands and the very small dispersions indicate that the σ-CDW state is an insulator.

Inspection of the 293 K band structure (Figure 5a), makes clear that the metallic character is confined to the [0 0 1] direction because the Fermi level lies at $E_F = -8.48$ eV, which is right at the top of the valence band along the [0 1 0] direction. Nevertheless, the bottom of the conduction band along [0 1 0] lies at -8.41 eV and thus the energy gap is small and the vacant orbitals can configurationally mix into the ground state in a continuous manner so as to drive the observed equilibrium between the π-chain-RVB radical ($P2/c$) and σ-dimer-CDW ($P2_1/c$) structures. In fact, according to the EHT band structures the energy gap along [0 1 0] is less than 0.1 eV at all temperatures. The unit cell volume contracts throughout the whole temperature range (Figure 2c), and between 293 and 15 K this contraction amounts to 3%, of which 2% comes from the shrinkage of the b unit cell parameter (Figure 2a). Nevertheless according to the EHT calculations, the energy gap between the valence and conduction bands along [0 1 0] in the RVB phase is almost invariant to temperature [0.07 (293 K) and 0.08 eV (15 K)] so we are unable to satisfactorily rationalize the intrusion of the σ-dimer-CDW phase as the temperature is lowered, much less its retreat below 150 K.

The conductivity and magnetism are well explained by the structural and band structure information, as it may be seen that the drop in paramagnetism (Figure 4a) follows the incursion of the CDW phase (Figure 2d) which is expected to be diamagnetic.[32,53] Likewise the activation energy for the conductivity peaks when the fraction of the CDW phase reaches a maximum as this phase is expected to be insulating;[32,53] presumably in this region the remnant conductivity is due to percolating pathways composed of the RVB phase (see below). It will be of some interest to further investigate this region with techniques such as pressure.

Charge Density Wave State in 18. We have previously identified a number of π-CDW phases in the chalcogenide radicals, including neutral systems in which the average number of carriers per lattice site (ρ), is given by $\rho = 1$,[9,10] and a doped neutral radical phase in which $\rho = 3/8$.[72,73] The distinctive features associated with compound **18** include the occurrence of the σ-CDW state that competes with an RVB conducting phase over an extremely broad temperature range and which develops as a nonmonotonic function of temperature.

The charge density wave (CDW) state is usually associated with pseudo one-dimensional (1-D) metals which are unstable to a lattice distortion as a result of the fact that there always exists a periodic modulation of the electron density distribution that lowers the electronic energy and produces a gap (Δ) in the density of states.[74,75] The resulting collective mode is associated with the wave vector $q = 2k_f$ and the wavelength (λ) of the lattice distortion is related to the Fermi wave vector (k_f) as shown in eq 1.

$$\lambda = \frac{\pi}{k_f} \tag{1}$$

The wave vector of the lattice distortion is given by

$$q = 2k_f = \rho\frac{\pi}{b} \tag{2}$$

where ρ is the number of carriers per site and b is the lattice constant (Table 1 and Figure 3a); for the half-filled band case ($\rho = 1$)

(72) Bryan, C. D.; Cordes, A. W.; Fleming, R. M.; George, N. A.; Glarum, S. H.; Haddon, R. C.; Oakley, R. T.; Palstra, T. T. M.; Perel, A. S.; Schneemeyer, L. F.; Waszczak, J. V. *Nature* **1993**, *365*, 821–823.
(73) Bryan, C. D.; Cordes, A. W.; Fleming, R. M.; George, N. A.; Glarum, S. H.; Haddon, R. C.; MacKinnon, C. D.; Oakley, R. T.; Palstra, T. T. M.; Perel, A. S. *J. Am. Chem. Soc.* **1995**, *117*, 6880–6888.
(74) Berlinsky, A. J. *Rep. Prog. Phys.* **1979**, *42*, 1243–1283.
(75) Gruner, G. *Rev. Mod. Phys.* **1988**, *60*, 1129–1181.

$$q = 2k_f = \frac{\pi}{b} \quad (3)$$

and

$$\lambda = 2b \quad (4)$$

As each of the radical molecules **18** possesses 1 unpaired electron, the doubling of the lattice constant along *b* is in accord with expectations (Table 1 and Figure 3a). However, there are a number of aspects of the structure and properties of the CDW state of **18** that are highly unusual, and we raise some of these points below.

The resonating valence bond (RVB, space group $P2/c$) and σ-charge density wave (σ-CDW, $P2_1/c$) phases coexist over a temperature range of more than 275 °C, and we are not aware of any other case where the CDW state does not constitute the low temperature ground state. This is particularly unusual for the exactly half-filled band case which is the most strongly driven of the CDW distortions and the fact that the transition involves a very large change in the C···C separations (from 3.22 Å in the RVB structure to 1.62 and 3.26 Å in the σ-CDW structure, Figure 2), argues for a strong energetic preference among the phases. There does not seem to be any hysteresis associated with the phase transition even though this is usually observed with dynamic σ-dimers[67] (excluding the fullerenes[60−62] and diazaphenalenyl[25]); in fact most σ-dimers are static.[32,53]

We considered the possibility that the conductivity in the region of maximum occupancy of the σ-CDW state (115 to 175 K), might be due (in part) to motion of the charge density wave even though highly commensurate CDWs are not expected to slide because of their strong pinning to lattice defects and impurities.[76,77] We did not notice any nonlinearity in the current−voltage scans and thus we conclude that if current is transported by sliding CDWs it does not exhibit a depinning voltage threshold. As noted by Lee, Rice and Anderson (LRA)[76,77] when the coherence length of the ordering becomes too long, the sliding electron lattice is pinned by one of the following phenonemena: (a) commensurability energy, (b) three-dimensional ordering, or (c) "sticking" at impurities. They note that the first two will give sharp, the last gradual transitions to a low-temperature insulating state with a large dielectric constant caused by the relatively weakly pinned sliding mode. In our case the first two factors are strongly developed (although we have a 2-dimensional material), and thus sliding CDWs are not expected. We would also expect a sharp transition to the CDW state which is clearly not observed (Figure 3). However as noted by LRA,[76,77] the CDW state is critically dependent on impurities and lattice defects and this is reflected in the onset of the transition and degree of perfection achieved in the new low symmetry lattice. In the present case this behavior is evident in the data given in the Supporting Information which shows the sensitivity of the conductivity and magnetism to the regularity of the crystals under study (Figures S4−S7, Supporting Information).

The low temperature magnetic susceptibility is dominated by Curie spins which occur in high and variable concentration in the lattice of **18** (Figure S4, Supporting Information). While some of these spins are undoubtedly due to lattice defects, it seems likely that a significant fraction arises from solitons that are trapped in the lattice by out-of-phase degenerate domains of the σ-CDW state.[67,78−80] In the present case, the neutral solitons will be contained in extremely narrow domain walls and perhaps confined to a single lattice constant; suggesting their strong localization.[78,81]

Conclusion

We have synthesized and characterized a new phenalenyl-based neutral radical conductor; among the remarkable properties of this material − some of which are without precedent − we note the following: (1) resonating valence bond (RVB, space group $P2/c$) and σ-charge density wave (σ-CDW, $P2_1/c$) phases dynamically compete for structural occupancy between 15 and 293 K, (2) the entrance of the σ-CDW is gradual and it achieves a structural occupancy of about 60% at 150 K, but ultimately fails to annihilate the RVB phase which again predominates at 15 K, (3) in the region of maximum occupancy of the σ-CDW phase (115 to 175 K), where the structure is solved in the $P2_1/c$ space group, the paramagnetic susceptibility and the conductivity remain finite, and (4) the activation energy of the conductivity peaks in this region ($E_a = 0.55$ eV at 155 K), but recovers its original value of $E_a \approx 0.1$ eV below 100 K.

Experimental Section

Materials. All reactions and manipulations were carried out under an atmosphere of dry argon using standard Schlenk and vacuum-line techniques. 2-Methoxynaphthalene (Aldrich), benzoyl chloride (Acros), anhydrous aluminum chloride (Aldrich), benzylamine (Aldrich), boron trichloride (Aldrich), sodium tetraphenylborate (Aldrich), tetrakis(dimethylamino)ethylene (TDAE, Aldrich) and cobaltocene (Strem) were used as received. 6-Hydroxy benzanthrone was synthesized according to a modification of the literature method.[46] Solvents were dried and distilled according to standard procedures immediately before use. The NMR spectra were recorded on a Bruker 300 spectrometer. Mass spectra (MALDI) were run on a Voyager-DE STR BioSpectrometry Workstation mass spectrometer. Elemental analyses were performed by the Microanalysis Laboratory, University of Illinois, Urbana, IL.

Preparation of 6-Hydroxy-benzo[de]anthracen-7-one (19). 2-Methoxynaphthalene (31.6 g, 0.20 mol) and benzoyl chloride (24 mL, 0.20 mol) were dissolved in 150 mL of 1,2-dichlorobenzene and the mixture cooled in an ice bath. Aluminum chloride (106.6 g, 0.80 mol) was added slowly in four batches at intervals of half an hour; the reaction was heated to 140 °C for 48 h, cooled to room temperature and quenched with 600 mL 6 N hydrochloric acid. The slurry was filtered through Celite and washed with 400 mL methylene chloride. The organic layer was separated and washed repeatedly with water and then dried over sodium sulfate. The solvent was removed under reduced pressure to give a black solid. The crude material was purified by column chromatography (silica gel, 400 mesh) using chloroform. The solid obtained after evaporation of the solvent was recrystallized from a methanol and dichloromethane mixture gives 28 g (57%) of yellow crystalline solid. mp 180−181 °C (lit. 180.1−180.6 °C);[46] ^{1}H NMR (300 MHz, $CDCl_3$, 25 °C): δ 15.77 (1H, s), 8.54 (1H, d, $J = 8.4$ Hz), 8.46 (1H, d, $J = 7.7$ Hz), 8.35 (1H, d, $J = 8.2$ Hz), 8.05 (1H, d, $J = 9.0$ Hz), 7.87 (1H, d, $J = 7.9$ Hz), 7.76 (1H, t, $J = 8.4$ Hz), 7.60 (1H, t, $J = 7.0$ Hz), 7.54 (1H, t, $J = 7.8$ Hz), 7.25 (1H, d, $J = 9.0$ Hz); ^{13}C NMR (75 MHz, $CDCl_3$, 25 °C): δ 169.83, 139.72, 133.18, 130.66, 127.69, 126.93, 125.27, 123.96, 122.94, 120.22 ppm; ESI-

(76) Lee, P. A.; Rice, T. M.; Anderson, P. W. *Phys. Rev. Lett.* **1973**, *31*, 462–465.
(77) Lee, P. A.; Rice, T. M.; Anderson, P. W. *Solid State Commun.* **1974**, *14*, 703–709.
(78) Su, W. P.; Schrieffer, J. R.; Heeger, A. J. *Phys. Rev. Lett.* **1979**, *42*, 1698–1701.
(79) Bredas, J.-L.; Street, G. B. *Acc. Chem. Res.* **1985**, *18*, 309–315.
(80) Heeger, A. J. *Phil. Trans. Roy. Soc. (London) A* **1985**, *314*, 17–35.
(81) Pople, J. A.; Walmsley, S. H. *Mol. Phys.* **1962**, *5*, 15–20.

MS: *m*/*z* calcd for $C_{17}H_{11}O_2$ [MH^+], 247.0754, found 247.0759; Anal. Calcd (found) for $C_{17}H_{10}O_2$: C, 82.91 (82.60); H, 4.09 (3.91).

Preparation of 6-Benzylamino-benzo[de]anthracen-7-one (20). A mixture of 6-hydroxybenzanthrone (4.92 g, 0.02 mol) and benzylamine (15 mL) were heated to 185 °C in a heavy-walled sealed tube for 48 h. The mixture was allowed to cool, the tube was vented and opened, and the contents poured into 50 mL of distilled water. The aqueous mixture was extracted with 200 mL chloroform. The organic layer was washed repeatedly with water and dried over anhydrous sodium sulfate. The solvent was removed under reduced pressure to give red oil. The crude product was purified by column chromatography on Al_2O_3 with $CHCl_3$ to give a yellow solid. Recrystallization from a methanol and dichloromethane mixture gave 4 g (60%) of the desired compound. mp 190 °C; ^{1}H NMR (300 MHz, $CDCl_3$, 25 °C): δ 12.41 (1H, s), 8.69 (1H, d, $J = 7.9$ Hz), 8.56 (1H, d, $J = 7.7$ Hz), 8.45 (1H, d, $J = 8.1$ Hz), 7.87 (1H, d, $J = 9.3$ Hz), 7.78 (1H, d, $J = 8.0$ Hz), 7.74 (1H, t, $J = 8.4$ Hz), 7.61 (1H, t, $J = 7.5$ Hz), 7.50−7.29 (6H, m), 7.10 (1H, d, $J = 9.3$ Hz), 4.76 ppm (2H, d, $J = 5.9$ Hz); ^{13}C NMR (75 MHz, $CDCl_3$, 25 °C): δ 155.45, 138.40, 131.49, 130.19, 128.92, 127.53, 127.22, 127.10, 126.93, 124.91, 122.57, 122.03, 114.43, 46.81; ESI-MS: *m*/*z* calcd for $C_{24}H_{18}NO$ [MH^+] 336.1388; found, 336.1389; Anal. Calcd (found) for $C_{24}H_{17}NO$: C, 85.94 (85.48); H, 5.11 (4.98); N, 4.18 (4.18).

Preparation of Bis(6- benzylamino-7-oxo-benz-anthracene)boron Tetraphenylborate ($18^+BPh_4^-$). A mixture of 6-*N*-benzylamino-7-oxo-benzanthracene (0.67 g, 2 mmol) and triethylamine (0.20 g, 2 mmol) in dry dichloromethane (40 mL) was treated with boron trichloride (1 M solution in hexane) under argon. The mixture was stirred for 72 h at room temperature. The yellow solution of the ligand became dark red in color upon addition of boron trichloride. Solid sodium tetraphenyl borate (1.03 g, 3 mmol) was added and the reaction was stirred at room temperature. After 1 h the reaction was filtered and 20 mL of dry methanol was added to the filtrate. The mixture was allowed to stand and after three days 0.45 g (45%) of a red crystalline salt was isolated by filtration and washed with methanol and ether. mp 222 °C; ^{1}H NMR (300 MHz, CD_3CN, 25 °C): δ 8.82 (1H, d, $J = 8.0$ Hz), 8.51 (1H, d, $J = 7.2$ Hz), 8.35 (1H, d, $J = 9.6$ Hz), 8.23 (2H, d, $J = 7.4$ Hz), 7.95 (1H, t, $J = 7.7$ Hz), 7.45 (1H, t, $J = 7.5$ Hz), 7.36 (1H, t, $J = 7.6$ Hz), 7.31−7.24 (6H, m), 7.17−7.06 (4H, m), 7.00 (4H, t, $J = 7.6$ Hz), 6.84 (2H, t, $J = 7.8$ Hz), 4.85 (1H, d, $J = 17.0$ Hz), 4.75 (1H, d, $J = 17.1$ Hz); MALDI-MS: *m*/*z* calcd for $C_{48}H_{32}BN_2O_2$ 679.2551 [M^+]; found 679; Anal. Calcd (found) for $C_{72}H_{52}B_2N_2O_2.CH_2Cl_2$: C, 80.90 (81.05); H, 5.02 (4.84); N, 2.58 (2.46).

Crystallization of Bis(6-benzylamino-7-oxo-benz-anthracene)-boron Radical (18). A solution of 40 mg (4.0×10^{-5} mol) of $18^+BPh_4^-$ in 20 mL of dry acetonitrile was placed in a container (25 mL round-bottom flask), and 25 mg (12×10^{-5} mol) of TDAE taken in 20 mL of dry acetonitrile was placed in another container (25 mL round-bottom flask). The containers were attached to an invertible H-cell in the glovebox. The H-cell was removed from the glovebox and inverted slowly. The solutions were allowed to diffuse through the glass frit. After sitting in the dark for 15 days, the cell yielded 19 mg (Yield 70%) of black shining crystals; 247 °C (decomposition temperature). ESI-MS: *m*/*z* calcd for $C_{48}H_{32}BN_2O_2$ 679.2551 [M^+]; found 679.2554; Anal. Calcd (found) for $C_{48}H_{32}BN_2O_2$: C, 84.83 (84.27); H, 4.75 (4.72); N, 4.12 (4.44).

Cyclic Voltammetry. Electrochemical measurements were performed using a CH Instruments Electrochemical Analyzer, with scan rates of 100 mV/s on solutions (10^{-3} M) of $18^+BPh_4^-$ in oxygen-free acetonitrile (distilled from CaH_2) containing 0.1 M tetra-*n*-butylammonium hexafluorophosphate. Potentials were scanned with respect to the saturated calomel reference electrode in a single-compartment cell fitted with Pt electrodes and referenced to the Fc/Fc^+ couple of ferrocene at 0.38 V vs SCE.

X-ray Crystallography. A black prismatic fragment ($0.39 \times 0.35 \times 0.26$ mm^3) of **18** was used for the single crystal X-ray diffraction study of $C_{48}H_{32}BN_2O_2$ at the following temperatures: 100, 110, 115, 125, 140, 150, 165, 175, 185, 200, 250, 270, and 293 K (low-temperature Bruker Kryoflex system, Bruker-AXS, Inc., UCR) For the 15K data set the crystal size was $0.10 \times 0.30 \times 0.30$ mm^3 (Cyrocool-LHe Cryogenic System, Cryo Industries of America, Argonne). X-ray intensity data were collected on a Bruker APEX2[82] platform-CCD X-ray diffractometer system (Mo-radiation, $\lambda = 0.71073$ Å, 50 KV/40 mA power). The CCD detector was placed at a distance of 5.000 cm (15 K data) and 5.0670 cm (all other data) from the crystal.

A total of 2400 frames were collected for a hemisphere of reflections, with scan width of 0.3° in ω, starting ω and 2θ angles at −30°, and ϕ angles of 0, 90, 180, and 270° for every 600 frames, 30 s/frame at 293 and 150 K, 15 s/frame at 15 K, and 10 s/frame at all other temperature. Based on a monoclinic crystal system, the frames were integrated using the Bruker SAINT software package[83] using a narrow-frame integration algorithm. Absorption corrections were applied to all the raw intensity data using the SADABS program.[84]

The Bruker SHELXTL software package[85] was used for phase determination and structure refinement. The distribution of intensities and systematically absent reflections indicated the *P*2/*c* (#13) space group for 15, 100, 110,175, 185, 200, 250, 270, 293 K data, and *P*2(1)/*c* (#14) space group for 115, 125, 140, 150, 165 K data. Direct methods of phase determination followed by two Fourier cycles of refinement led to an electron density map from which most of the non-hydrogen atoms were identified in the asymmetry unit of the unit cell. With subsequent isotropic refinement, all of the non-hydrogen atoms were identified. The SADI, DFIX, SIMU, DELU, and EADP restraints were applied to stabilize the refinement of the σ-dimer of the superstructure and π-dimer substructure. A free variable parameter, FVAR, was used to determine the site occupancy factor for the π-dimer/σ-dimer ratios at the various temperatures. All data sets were refined to 0.75 Å resolutions (maximum 2θ angle of 56.56°). Detailed descriptions of the analysis and results are provided in the Supporting Information.

Magnetic Susceptibility Measurements. Magnetic susceptibility measurements on two separate batches (see Supporting Information) of **18** were performed over the temperature range 4−355 K on a George Associates Faraday balance operating at 0.5 T. The system was calibrated using Al and Pt NIST standards.

Conductivity Measurements. The single-crystal conductivity (σ), of **18** was measured for two crystals (Figure S5−S7, Supporting Information) in a four-probe configuration using in-line contacts which were attached with silver paint. The needle-like crystals were freely positioned on a sapphire substrate, and the electrical connections between the silver paint contacts on the crystal and the indium pads on the substrate were made by thin, flexible 25 μm diameter silver wires to relieve mechanical stress during thermal cycling of the crystal. The temperature dependence of the conductivity was measured in the range 319−65 K using a custom-made helium variable temperature probe with a Lake Shore 340 temperature controller driven by LabVIEW software. A Keithley 236 unit was used as a voltage source and current meter, and two 6517A Keithley electrometers were used to measure the voltage drop between the potential leads in a four-probe configuration.

Band Structure Calculations. The band structure calculations made use of a modified version of the extended Huckel theory (EHT) band structure program,[86,87] as described previously.[32] The parameter set is chosen to provide a reasonably consistent picture of bonding in heterocyclic organic compounds.[10,88] The EHT calculations used a Gaussian smoothing factor ($\Delta = 0.02$ eV)[32] to

(82) *APEX 2*, 2009.5−1; Bruker AXS Inc.: Madison, WI, 2009.
(83) *SAINT*, V7.60A; Bruker AXS Inc.: Madison, WI, 2009.
(84) *SADABS*, 2008/1; Bruker AXS Inc.: Madison, WI, 2008.
(85) *SHELXTL*, 2008/4; Bruker AXS Inc.: Madison, WI, 2008.
(86) Hoffmann, R. *J. Chem. Phys.* **1963**, *39*, 1397–1412.
(87) Hoffmann, R. *Solids and Surfaces*; VCH: New York, 1988.
(88) Haddon, R. C.; Siegrist, T.; Fleming, R. M.; Bridenbaugh, P. M.; Laudise, R. A. *J. Mater. Chem* **1995**, *5*, 1719–1724.

obtain the DOS from k-point grids that were chosen on the basis of the Patterson space group.[89]

Acknowledgment. We thank Elena Bekayarova for helping to measure conductivity of the powder sample. Supported by the Office of Basic Energy Sciences, U.S. Department of Energy under grant no. DE-FG02-04ER46138 and by Argonne, a U.S. Department of Energy Office of Science Laboratory, operated under Contract No. DE-AC02-06CH11357.

Supporting Information Available: Additional structural information, magnetic susceptibility plot, crystal information, conductivity plots, conductivity activation energy plots, tables of atomic coordinates and CIF files for compounds **18** and $\mathbf{18}^{+}$ BPh_4^{-}; complete ref 25. This material is available free of charge via the Internet at http://pubs.acs.org.

JA908768A

(89) Ramirez, R.; Bohm, M. C. *Int. J. Quantum Chem.* **1988**, *34*, 571–594.